

USING REED-MULLER SEQUENCES AS DETERMINISTIC COMPRESSED SENSING MATRICES FOR IMAGE RECONSTRUCTION

Kangyu Ni¹, Somantika Datta², Prasun Mahanti³, Svetlana Roudenko¹, and Douglas Cochran¹

¹School of Mathematical and Statistical Sciences, Arizona State University

²Program in Applied and Computational Mathematics, Princeton University

³School of Electrical, Computer, and Energy Engineering, Arizona State University

ABSTRACT

An image reconstruction algorithm using compressed sensing (CS) with deterministic matrices of second-order Reed-Muller (RM) sequences is introduced. The 1D algorithm of Howard et al. using CS with RM sequences suffers significant loss in speed and accuracy when the degree of sparsity is not high, making it infeasible for 2D signals. This paper describes an efficient 2D CS algorithm using RM sequences, provides medical image reconstruction examples, and compares it with the original 2D CS using noiselets. This algorithm entails several innovations that enhance its suitability for images: initial best approximation, a greedy algorithm for the nonzero locations, and a new approach in the least-squares step. These enhancements improve fidelity, execution time, and stability in the context of image reconstruction.

Index Terms— Compressed Sensing, Reed-Muller Sequences, Image Reconstruction

1. INTRODUCTION

Compressive sensing (CS) methods are receiving attention in connection with reconstruction of pixelated images from projections onto sets of sampling vectors that are considerably smaller than the number of pixels in the image [4]. This is particularly true in regime of medical imaging (e.g., [7]), where certain modalities provide favorable levels of sparsity compared to natural images. This paper is primarily concerned with using second-order Reed-Muller (RM) sequences for deterministic compressed sensing in the imaging regime, especially for medical images. The starting point for this work is a 1D algorithm introduced by Howard et al. in [5], which requires several modifications to enable efficient and high-fidelity reconstruction of images.

If P is a $m \times m$ binary symmetric matrix and $a = (a_0, \dots, a_{m-1})^T$ and $b = (b_0, \dots, b_{m-1})^T$ are binary vectors in \mathbb{Z}_2^m , a second-order RM sequence of length 2^m is obtained

from these parameters by

$$\phi_{P,b}(a) = \frac{(-1)^{\text{wt}(b)}}{\sqrt{2^m}} i^{(2b+Pa)^T a}. \quad (1)$$

In this expression, $\text{wt}(b)$ is the weight of b , i.e., the number of ones in b . If P has zeros on the main diagonal, then $\phi_{P,b}$ is real-valued. The compressed sensing matrix discussed in [5] has the form

$$\Phi_{RM} = [U_{P_1} \ U_{P_2} \ \cdots \ U_{P_{2^{m(m-1)/2}}}], \quad (2)$$

where each U_{P_j} is a $2^m \times 2^m$ orthogonal matrix whose columns are the second-order RM sequences obtained by fixing P_j in (1) and letting b range through all possible binary m -vectors. Since there are $2^{m(m-1)/2}$ possible $m \times m$ binary zero-diagonal symmetric matrices, the associated full RM matrix has dimension $2^m \times 2^{m(m+1)/2}$. Defining $N = 2^{m(m+1)/2}$ and $n = 2^m$, a k -sparse signal $x \in \mathbb{C}^N$ yields a measurement $y = \Phi_{RM}x \in \mathbb{C}^n$, which is the superposition of k RM functions

$$y(a) = z_1 \phi_{P_1, b_1}(a) + z_2 \phi_{P_2, b_2}(a) + \cdots + z_k \phi_{P_k, b_k}(a). \quad (3)$$

In (3), the numbers z_j are the non-zero components of x and terms corresponding to the zeros in x are omitted. Note that P_j and b_j may individually repeat in the equation. To recover x , the deterministic reconstruction algorithm introduced in [5] uses the fast Hadamard transform (FHT) to detect the locations of the nonzero elements in x deduce the corresponding (P_j, b_j) pairs one-by-one. Its computational complexity is $O(kn(\log n)^2)$. The magnitudes z_j are then found by solving the associated least-squares problem. For reconstructing sparse signals, in terms of reconstruction speed and fidelity, this is more efficient than ℓ_1 minimization with random matrices, whose computational complexity is $O(knN)$.

Despite its efficacy in accurately reconstructing sparse 1D signals, applying this algorithm directly to images does not work well. This is because real images are not as sparse in any transform domain as the 1D signals in [5], and therefore, the reconstruction error becomes large. For example, a 128×128 image with 10% sparsity has 1638 nonzero coefficients. At

This work is partially supported by NSF-DMS grant #0652833, NSF-DUE #0633033, and ONR-BRC grant #N00014-08-1-1110.

least approximately 4000 measurements are needed in order for the reconstruction to be correct. This implies that only four P matrices in (2) are needed to solve $y = \Phi_{RM}x \in \mathbb{C}^{2^m}$, and therefore, the efficiency of finding nonzero locations is not fully utilized in the imaging regime. Moreover, the algorithm requires about 1638 iterations and the least-squares computations become onerous.

Section 2 of this paper describes a deterministic algorithm for compressed sensing and reconstruction of images using RM sequences. Section 3 presents results of experiments with 256×256 medical images and compares these with results obtained using noiselets, as described in [3]. Section 4 summarizes the results.

2. METHOD

2.1. Construction of the compressive sensing matrix

As explained in the introduction, due to the sparsity nature of images and rule of thumb in compressed sensing, only four P matrices are needed for the sensing matrix, instead of the entire matrix given in (2). Therefore, there is flexibility to construct the sensing matrix according to the choice of P matrices. The statistics of inner products of two columns, each of which is taken from U_{P_i} and U_{P_j} , respectively, are [8]

$$|\langle \phi_{P_i, \cdot}, \phi_{P_j, \cdot} \rangle| = \begin{cases} 1/\sqrt{2^l}, & 2^l \text{ times,} \\ 0, & 2^m - 2^l \text{ times,} \end{cases} \quad (4)$$

where $l = \text{rank}(P_i - P_j)$. If $l = m$, the inner products are always $1/\sqrt{2^m}$, which is smaller than if $l < m$. This is desirable because the nonzero locations are unknown and the inner products between any two columns are as small as possible. Since the rank between two zero-diagonal symmetric binary matrices is always even, m is even in this paper. The set of zero-diagonal symmetric binary matrices such that the rank between any two matrices is equal to m is called the Kerdock set [6]. There are 2^{m-1} elements in the Kerdock set, and the construction of the Kerdock set can be found in [2]. The sensing matrices used in this paper are constructed in the form

$$\Phi = [U_{P_1} \ U_{P_2} \ U_{P_3} \ U_{P_4}], \quad (5)$$

where P_1, P_2, P_3 , and P_4 can be any matrices from the Kerdock set. For example, the sensing matrix for a 256×256 ($= 2^{16}$) image is of the size $2^{14} \times 2^{16}$. Therefore, only 25% of the measurements are sampled.

2.2. Initial best approximation of the solution

We propose a method to detect a large portion of the nonzero locations in one step, based on the knowledge from Fourier analysis that the energy of the wavelet coefficients is concentrated in the upper-left region. This does not require *a priori* knowledge of individual images. Write the measurements as

$$\begin{aligned} y = \Phi x &= [U_{P_1} \ U_{P_2} \ U_{P_3} \ U_{P_4}] \begin{bmatrix} x_1 \\ x_2 \\ x_3 \\ x_4 \end{bmatrix} \\ &= U_{P_1}x_1 + U_{P_2}x_2 + U_{P_3}x_3 + U_{P_4}x_4, \end{aligned} \quad (6)$$

where x_1, x_2, x_3 , and x_4 are vectors of the upper-left, lower-left, upper-right, and lower-right coefficients, respectively. The initial approximation estimates x_1 by observing

$$U_{P_1}^T y = x_1 + U_{P_1}^T U_{P_2} x_2 + U_{P_1}^T U_{P_3} x_3 + U_{P_1}^T U_{P_4} x_4. \quad (7)$$

The last three terms are small because x_2, x_3 , and x_4 are much sparser and smaller than x_1 , and the rest of the terms $U_{P_1}^T U_{P_2} x_2, U_{P_1}^T U_{P_3} x_3$, and $U_{P_1}^T U_{P_4} x_4$ are small, as discussed in Sec. 2.1. Therefore, $U_{P_1}^T y \approx x_1$. In the case when all nonzero locations are in the upper-left region, i.e., x_2, x_3 , and x_4 are zero, $U_{P_1}^T y$ is equal to x_1 , which automatically completes the image reconstruction.

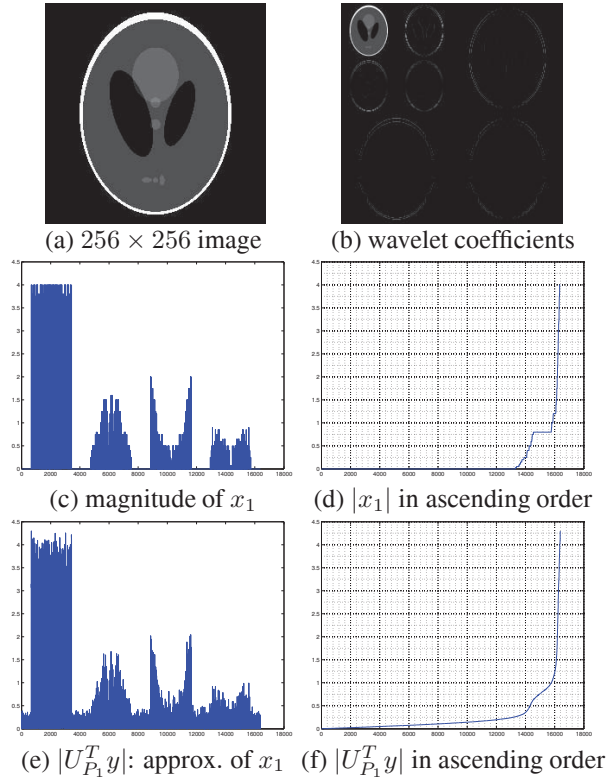


Fig. 1. In (b) it is shown the energy of wavelet coefficients is concentrated in the upper-left region; (c) and (e) show that $|U_{P_1}^T y|$ approximates $|x_1|$ well; (d) is the plot of $|x_1|$ sorted in ascending order, and finally, (f) is $|U_{P_1}^T y|$ in ascending order.

Fig. 1 shows an example of this method, where (a) is the Shepp-Logan phantom image of pixel resolution 256×256 and (b) shows its Haar wavelet coefficients. In (c) and (e), we see that $U_{P_1}^T y$ well approximates x_1 . Therefore, even though x_1 is unknown, most of the nonzero locations in x_1 can be

detected. The graph in (f) sorts the magnitudes of the approximation in ascending order. Most of the nonzero locations in x_1 can be detected by selecting the locations above the first critical point from the origin. In (f), such a critical point is around 14000. Denoting the detected locations by $(P_l, b_l), l = 1, \dots, j$, the magnitudes z_l can be well estimated by solving the following linear squares problem:

$$\min_z \|Az - y\|, \quad (8)$$

where A is the matrix whose columns consist of ϕ_{P_l, b_l} and $z = [z_1, \dots, z_j]^T$. The pseudo-inverse solution of (8) is

$$z_{sol} = (A^*A)^{-1}A^*y, \quad (9)$$

where $*$ is conjugate transpose. Since $P_l = P_1$ in the initial step, the solution is $z = A^*y$. Finally, subtracting the linear (their respective magnitudes z_l) sum of the found columns from y gives the residual, $y_0(\ell) = y(\ell) - \sum_{l=1}^j z_l \phi_{P_l, b_l}(\ell)$.

2.3. Reconstruction algorithm

This section describes the proposed method, which is summarized in the following steps:

1. Get initial best approximation (see Sec. 2.2).
2. Find multiple (P_l, b_l) pairs.
3. Determine z_j by updated linear least squares solutions.
4. Get residual $y_0(\ell) = y(\ell) - \sum_{l=1}^j z_l \phi_{P_l, b_l}(\ell)$.
5. Repeats steps 2–4 until y_0 is sufficiently small.

The second step first “de-chirps” the samples residual with all four P matrices in the measurement matrix, i.e., multiplication by $\overline{\phi_{P_j, 0}}$ eliminates the quadratic term, and then use the FHT to detect the remaining nonzero locations:

$$w_{P_j}(\ell) = \left| \text{FHT} \left(y_0(\ell) \overline{\phi_{P_j, 0}(\ell)} \right) \right|, \quad j = 1, 2, 3, 4. \quad (10)$$

Each obtained magnitude corresponds to a unique pair (P_j, ℓ) . The largest magnitudes are selected and the corresponding pairs give the nonzero locations.

The third step solves the magnitudes z_j using (8). The matrix A in the current step can be expressed as $A = [\tilde{A} \ c]$, where \tilde{A} is from the previous step and c is the newly found columns. To solve the least squares problems without treating each problem (iteration) independently, we use an updated pseudo inverse solution method whose computation is based on previous calculations.

To obtain (9), first finding the inverse of

$$A^*A = \begin{bmatrix} \tilde{A}^* \tilde{A} & \tilde{A}^* c \\ c^* \tilde{A} & c^* c \end{bmatrix} \quad (11)$$

can be made efficiently by the Schur-Banachiewicz blockwise inversion formula (e.g., see [1]):

$$\begin{bmatrix} D & E \\ F & G \end{bmatrix}^{-1} = \begin{bmatrix} D^{-1} + D^{-1}EVFD^{-1} & -D^{-1}EV \\ -VFD^{-1} & V \end{bmatrix}, \quad (12)$$

where $V = (G - D^{-1}E)^{-1}$. Note that D^{-1} is known from the previous iteration and the size of $V = (G - D^{-1}E)^{-1}$ is small. A^*y can also be updated by only calculating c^*y , in which the size of c is much smaller than the size of A .

3. RESULTS

In these experiments, each original image was sparsified by computing its Haar wavelet transform and retaining a pre-determined fraction of its wavelet coefficients, keeping the largest and setting the rest to zero. Then, 25% noiselet measurements and RM measurements were taken for noiselet and RM reconstruction, respectively. Fig. 2 (a) is the 256×256 vessel image with 10% sparsity. The reconstructed image using (our implementation of) Candès and Romberg’s method with noiselets [3] is shown in (b), which has noticeable patches. The reconstructed image in (c) is by our method and is identical to the reference image in (a). In (b), (d), and (f), the respective horizontal slices at the center are shown and the slice by our method is identical to the slice in the reference image. The reconstruction error by our method (-283 dB), is notably better than the error by noiselets (-19 dB), where the error is defined as:

$$\text{Error(dB)} = 10 \log_{10} \left[\frac{\|x_{\text{actual}} - x_{\text{reconstructed}}\|^2}{\|x_{\text{actual}}\|^2} \right]. \quad (13)$$

Fig. 3 shows image reconstruction for the 256×256 MRI knee image. The true image is 10%-sparse and 25% samples were used for reconstruction. Our method in this case also outperformed the noiselet method. The error for RM was -284 dB, whereas the error for noiselets was -22 dB.

Table 1 shows reconstruction error in dB for various 256×256 images, using 25% measurements by the proposed algorithm. The reconstruction works well up to around 10%.

Sparsity	vessel	knee	phantom	cameraman
6%	-288	-289	-286	-289
7%	-287	-288	-286	-287
8%	-286	-286	-285*	-286
9%	-284	-285	N/A	-282
10%	-283	-284	N/A	-32

Table 1. Our method accurately reconstructs images with sparsity up to around 10% with only 25% measurements. *The phantom image is 7.27% sparse.

4. CONCLUSION

We have proposed a new image reconstruction algorithm for the deterministic compressed sensing method especially suitable for medical images. Compared to compressed sensing reconstruction from noiselets, this algorithm provides

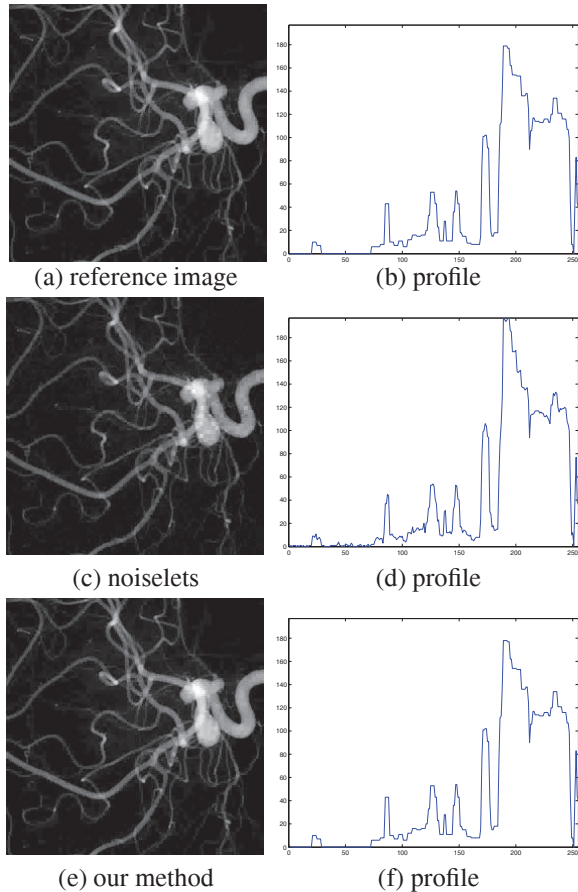


Fig. 2. (a) 256×256 vessel image with 10% sparsity. (c) reconstructed image with noiselets, error is -19 dB. (e) reconstructed image with our method, whose error is smaller, -283 dB. The respective horizontal slices in (b), (d), and (f) also show our result is identical to the reference image.

improved reconstruction in terms of error (SNR) and computational efficiency. New aspect of the algorithm include an initial best approximation step, which speeds up the solution and significantly decreases error (the proof is not shown due to space limitation), as can be observed in the examples shown. The total computational complexity of finding nonzero locations in the iterative step in our experiments is $O(\frac{1}{5}kn \log n)$, which is much smaller than $O(kn(\log n)^2)$ for the algorithm in [5] on the same size problem. Finally, an “updated least squares method” is incorporated to increase computational efficiency and stability.

5. ACKNOWLEDGMENTS

The authors wish to thank Robert Calderbank, Stephen Howard, and Stephen Searle for discussions about Reed-Muller codes and Jim Pipe for providing the medical images.

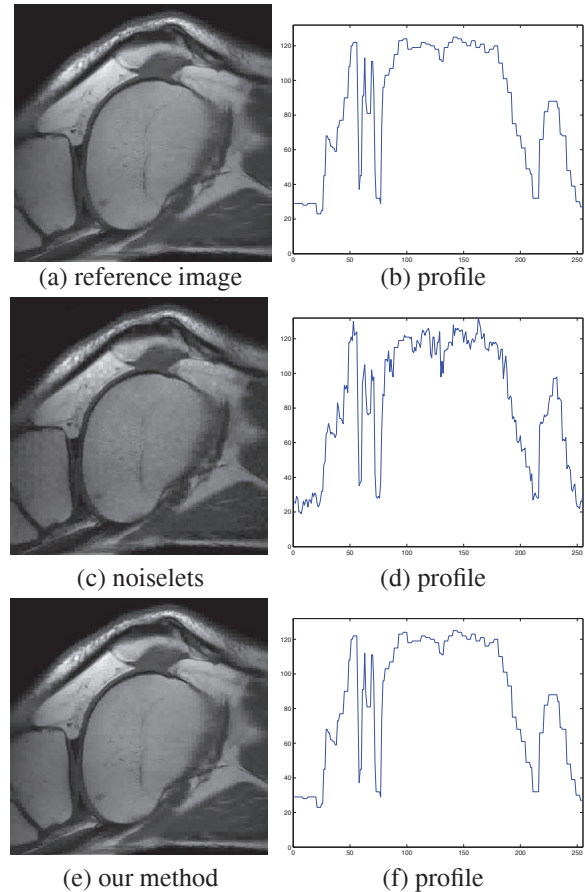


Fig. 3. (a) 256×256 knee 10%-sparse image. (c) reconstructed image with noiselet, error = -22 dB. (e) reconstructed image with our method. The error is much smaller, -284 dB. The respective horizontal slices in (b), (d), and (f) also show our result is identical to the reference image.

6. REFERENCES

- [1] A. Björck, *Numerical methods for least squares problems*, SIAM, 1996.
- [2] A. R. Calderbank, personal communication, 2009.
- [3] E. Candès and J. Romberg, “Sparsity and incoherence in compressive sampling,” *Inverse Problems* **23**(3), 969 – 985, 2007.
- [4] N. Dobigeon, A. O. Hero, and J.-Y. Tourneret, “Hierarchical Bayesian sparse image reconstruction with application to MRFM,” *IEEE Trans. Image Proc.* **18**(9), 2059–2070, 2009.
- [5] S. D. Howard, A. R. Calderbank, and S. J. Searle, “A fast reconstruction algorithm for deterministic compressive sensing using second order Reed-Muller codes,” *Proc. of Conf. on Information Sciences and Systems*, 2008.
- [6] A. M. Kerdoock, “A class of low rate nonlinear binary codes,” *Information and Control* **20**, 182 – 187, 1972.
- [7] M. Lustig, D. L. Donoho, and J. M. Pauly, “Sparse MRI: The application of compressed sensing for rapid MR imaging,” *Magnetic Resonance in Medicine* **58**(6), 1182-1195, 2007.
- [8] F. J. MacWilliams and N. J. A. Sloane, *The theory of error correcting codes*, Elsevier, 1976.